Concept design of a greenhouse cooling system using multi-stage nanofiltration for liquid desiccant regeneration

Pasqualin, P.; Davies, P.a.

DOI:
10.1016/j.applthermaleng.2022.119057

Document Version
Publisher's PDF, also known as Version of record

Citation for published version (Harvard):
Pasqualin, P & Davies, PA 2022, 'Concept design of a greenhouse cooling system using multi-stage nanofiltration for liquid desiccant regeneration', *Applied Thermal Engineering*, vol. 216, 119057. https://doi.org/10.1016/j.applthermaleng.2022.119057

Applied Thermal Engineering 216 (2022) 119057

Contents lists available at ScienceDirect

Applied Thermal Engineering

journal homepage: www.elsevier.com/locate/apthermeng

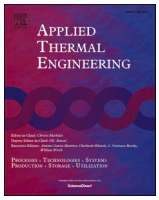

Research Paper

Concept design of a greenhouse cooling system using multi-stage nanofiltration for liquid desiccant regeneration

P. Pasqualin, P.A. Davies *

School of Engineering, University of Birmingham, Edgbaston, Birmingham B15 2TT, UK

ARTICLE INFO

Keywords:
Liquid desiccant air conditioning
Multi-stage regenerator
Greenhouse cooling

ABSTRACT

Liquid desiccant air conditioning (LDAC) has been proposed for greenhouse cooling. LDAC achieves lower temperatures than conventional evaporative cooling while also allowing closed air recirculation which has advantages over open ventilation. However, liquid desiccant regeneration is challenging and energy intensive. A novel multi-stage nanofiltration (NF) system is proposed as a regeneration method to enable both greenhouse cooling and irrigation in a closed water cycle. This concept study shows that, during winter and summer respectively, a 9-stage NF regenerator recovers 4.8 and 6.6 L of water per day per m^2 of greenhouse floor area. Using commercial NF membranes with burst pressures of ~ 40 bar, a 9-stage regenerator using $CaCl_2$ could achieve a yearly *COP* of ~ 12.4 and monthly greenhouse temperatures below 32 °C, almost independent of location. This improves greatly on LDAC using open evaporative regenerators, which only provides a *COP* of 0.3–0.5. Future research allowing NF membranes to operate with burst pressures of 55 bar could achieve the same *COP* by using just a 4-stage regenerator, making the system less expensive and more compact. Perspectives on the proposed design and implementation are discussed. This study shows the potential of the multi-stage NF regenerator to cool greenhouses in hot climates where it is difficult to produce crops during summer.

1. Introduction and motivation

Greenhouses in hot climates often struggle to produce crops during summer because the temperature inside the greenhouse rises above the acceptable range for cultivation [1]. To enable cultivation year-round, cooling technologies are needed, but conventional cooling technologies such as vapour compression and evaporative cooling have significant downsides. Vapour compression requires large amounts of energy and typically utilises refrigerants that contribute to global warming; and evaporative cooling is only suitable for locations with abundant supplies of water. Therefore, resource-efficient greenhouses are not yet available for hot climates with limited water availability [2]. To address this important gap, there is a need for improved thermal processes with low water demands.

Liquid desiccant air conditioning (LDAC) has the potential to replace conventional cooling because it is more energy efficient and environmentally friendly [3], and allows storage of the liquid desiccant (LD) for use when needed [4]. Another advantage is that LDAC provides simultaneous cooling and dehumidification.

Dehumidification is especially important for greenhouses, where crops continually release water vapour by transpiration [5]. Because of transpiration, the cooling system must remove large amounts of vapour, especially when operated in closed recirculation. Closed air recirculation has several advantages over open ventilation, usually resulting in higher quality and yield of crop [6]. Moreover, it allows CO_2 enrichment without loss of CO_2 to the surroundings; and it protects against insects and pests [6]. Closed operation can also decrease energy and water demands [6]. Therefore, closed air recirculation is preferred in this study.

For effective absorption of vapour using LDAC, high LD concentrations should be used [7,8]. The absorbed moisture must be removed from the LD in a process called regeneration [9]. LDAC presents several challenges, but the high energy requirement of regeneration is the most critical [10]. Some early studies focused on open evaporative regenerators, but this is an energy-intensive and inefficient approach [11]. For example, one study found that open evaporative regenerators would occupy an area up to four times the floor area of the greenhouse [12]. Therefore, there is a need for more efficient and compact LD regeneration.

Membrane-based desalination technologies have been proposed as alternative LD regenerators. These technologies include membrane

* Corresponding author.
E-mail address: P.A.Davies@bham.ac.uk (P.A. Davies).

https://doi.org/10.1016/j.applthermaleng.2022.119057
Received 10 March 2022; Received in revised form 19 July 2022; Accepted 21 July 2022
Available online 25 July 2022

Nomenclature[11]

ERD	Energy recovery device
LD	Liquid desiccant
LDAC	Liquid desiccant air conditioning
NF	Nanofiltration
PV	Photovoltaic
RO	Reverse osmosis

Parameters

A	Area [m^2]
C	Concentration [g/L] {g/dm^3}
COP	Coefficient of performance [-]
c_p	Heat capacity [kJ/(kg K)]
ET	Crop transpiration rate [kg/s]
h	Heat loss coefficient [$kW/(m^2\ K)$]
I	Solar radiation [kW/m^2]
k_c	Crop coefficient [-]
LAI	Leaf area index [$m^2/\ m^2$]
M	Molar mass [g/mol]
$\dot{m}$	Mass flow [kg/s]
P	Electric power [kW]
P_{vap}	Vapour pressure [kPa]
$\dot{Q}$	Exchanged heat [kW]
r	Rejection [-]
r_a	Aerodynamic external resistance [s/m]
r_c	Internal resistance of the canopy [s/m]
R	Universal gas constant [(L bar)/(K mol)] {(dm^3 MPa)/(10 K mol)}
RH	Relative humidity [%]
R_n	Radiation above the canopy [$kJ/(m^2\ h)$]
r_R	Radiative resistance [s/m]
SEC	Specific energy consumption [kWh_{el}/m^3] {3.6 MJ_{el}/m^3}
T	Temperature [°C] or [K]
U	Speed [m/s]
V'	Inverse of the pure water molarity [L/mol] {dm^3/mol}
$\dot{V}$	Flowrate [L/h] {$dm^3/(60\ s)$}
VPD	Vapour pressure deficit of the air [kPa]
W_{SP}	Specific work [kJ/kg]
wt	Weight concentration [wt.%]
x	Mass fraction [–]

Greek letters

α	Absorbance of greenhouse floor with crop [–]
α_w	water activity [–]
β	Fraction of roof area covered by PV collectors [–]
Δ	Slope of the saturation vapour pressure curve [kPa/K]
ΔP	Applied pressure [bar] {MPa/10}
$\Delta\Pi$	Osmotic pressure difference [bar] {MPa/10}
ε_{evap}	Effectiveness of the evaporative cooling pad [–]
η	Efficiency [–]
λ	Latent heat of evaporation [kJ/kg]
σ_{S-B}	Constant of Stefan–Boltzmann [$W/(m^2\ K^4)$]
τ	Roof transmittance [–]
ρ	Density [kg/m^3]
ω	Humidity ratio [g_v/kg_a]

Subscripts

Air	Air
amb	Ambient
b	Brine
c	Crop
CaCl2	Calcium chloride
cool	Cooled air leaving the dehumidifier
d	Dried air
end	Exit from the multi-stage regenerator
ERD	Energy recovery device
f	Feed
gh	Greenhouse
K	Kelvin degree
LD	Liquid desiccant
NF	Multi-stage NF regenerator
out	End of the greenhouse
p	Permeate
pump	Pump
pv	Photovoltaic
s	Surface
system	System
v	Moisture

Superscripts

amb	Ambient
deh	Dehumidifier
in	Inlet of the dehumidifier
out	Outlet from the dehumidifier

Energy and power units

kWh_{el}	Electric energy consumption [kWh] {3.6 MJ}
kW_{el}	Electric power consumption [kW]

distillation [13–17], reverse osmosis [18] and electrodialysis [19–23]. In general, membrane-based desalination technologies can be pressure-driven (such as reverse osmosis and nanofiltration) or thermally-driven (such as membrane distillation). Several studies found that pressure-driven are more efficient than thermally-driven membrane processes for seawater and brackish water desalination [24–26]. Therefore, it is reasonable to expect that pressure-driven membrane processes may also be more efficient for LD regeneration [27]. So far, however, the high concentrations of the LD have prevented the use of pressure-driven membrane processes for this purpose because the membrane burst pressure would be exceeded.

A possible solution is multi-stage nanofiltration (NF) systems. These systems are gaining interest as an energy-efficient membrane process for highly concentrated feeds. In contrast to reverse osmosis (RO), NF membranes can operate with a total osmotic pressure difference higher than the burst pressure of a single membrane. This is because NF membranes have lower rejections than commercial RO membranes (the rejection of which is about 98 % [28,29]), allowing NF membranes to gradually decrease the concentration of the LD via several stages. As a result, the total osmotic pressure is divided among the stages, thus allowing the osmotic pressure difference across each membrane to be lower than its burst pressure.

Though not yet used in LDAC, multi-stage NF systems have been investigated numerically for concentration of seawater. For example, Altaee and Sharif [30] modelled a 2–stage NF system and predicted permeate qualities of 0.254 and 0.359 g/L when treating seawater with concentrations of 35 and 43 g/L, respectively. More recently, Wang et al. [31] modelled a multi-stage NF system able to obtain highly concentrated brines suitable for crystallisation applications in zero liquid discharge systems. These authors studied a 3-stage system (consisting of an initial RO stage, followed by 2 NF stages and then an energy recovery device) which concentrated seawater feed at 60 g/L to give a brine at 233.3 g/L. They predicted a specific energy consumption (*SEC*) of 15.74 kWh_{el}/m^3 (electrical input per m^3 of water produced). They also

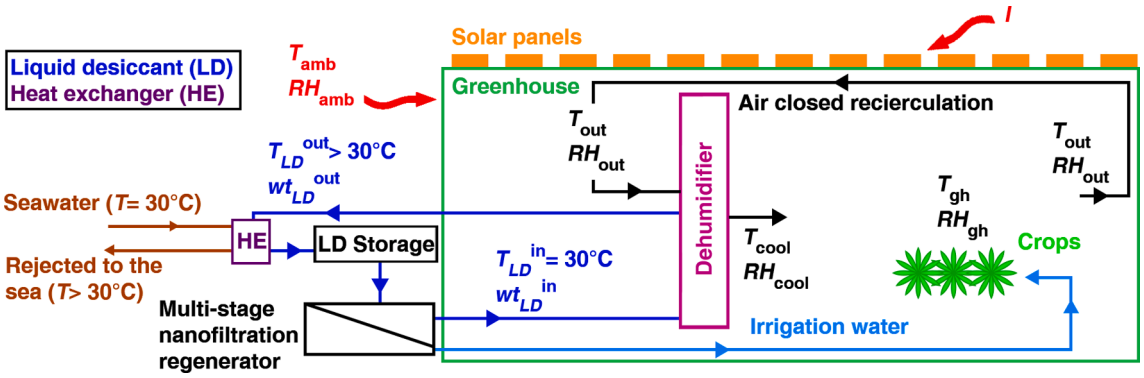

Fig. 1. Schematic of a greenhouse operating in closed air recirculation which regenerates the liquid desiccant (LD) using a multi-stage nanofiltration regenerator. The solar panels are assumed to be uniformly distributed on top of the greenhouse. The greenhouse absorbs heat from the air entering the dehumidifier and rejects this heat to the sea (assumed with a temperature (*T*) equal to 30 °C) through a liquid-to-liquid heat exchanger (HE). The names of the LD parameters are explained in Appendix B, while the other parameters are explained in section 3.

modelled a similar 4-stage system and predicted a *SEC* of 7.98 kWh_{el}/m^3, thus showing that *SEC* tended to decrease as more stages were added. These values of *SEC* are significantly lower than those expected in conventional mechanical vapour compression (MVC) desalination systems where *SEC* is expected to be in the range of 20–25 kWh_{el}/m^3 [32].

Although NF has not yet been experimentally investigated for the regeneration of highly concentrated LDs, it has been investigated using similar LD compounds at lower concentrations. Compounds considered as LDs include chlorides of magnesium, calcium and lithium. Thus, Afonso and de Pinho [33] investigated the transport of magnesium chloride ($MgCl_2$) across an amphoteric NF membrane and reported rejections in the range of 10–30 % using concentrations up to 1.05 wt%. Moreover, Murthy and Chaudhari [34] investigated the rejection by the NF-300 (fabricated by Applexion) membrane with solutions including calcium chloride ($CaCl_2$) and $MgCl_2$ at concentrations up to 1 wt%. The results showed that $CaCl_2$ rejection was between 70 and 80 %, while $MgCl_2$ rejection was between 80 and 90 %. Another study investigated the possibility of recovering lithium from brines using composite NF membranes with positively charged skin layers [35]. Rejections for Li, Mg and Cl were in the ranges of 0–40 %, 60–90 % and 60–90 %, respectively. The study also reported average lithium chloride (LiCl) and $MgCl_2$ rejections of 70 and 83 %, respectively, for LD concentrations of 0.2 wt%.

The above three studies showed that NF partially rejected LiCl, $CaCl_2$ and $MgCl_2$ which is the requirement for a multi-stage regeneration process. However, the concentrations were too low for LDAC applications [27]. It should be noted that, though lithium salts like LiCl and lithium bromide (LiBr) are often considered the best LD as they can absorb large amounts of moisture [36], they are also very toxic [37,38]. For this reason, this study prefers $CaCl_2$ as it has good dehumidification performance and is much less toxic [39].

The aim of this study is to propose and analyse a concept of a closed air recirculation greenhouse cooled by LDAC using a multi-stage NF regenerator. Whereas previous studies considered LDAC for greenhouses using less efficient means of regeneration [1,12,40,41], this study is novel in that it assesses the potential of the multi-stage NF regeneration to provide a compact and efficient solution.

The main location investigated in this study is Mecca (Saudi Arabia) with the Red Sea being the heat sink of the system. In total, three types of climates are considered – *hot and humid* (Mecca), *hot and arid* (Timbuktu), *semi-hot and semi-arid* (Cairo). Realistic climatic data for Mecca, Timbuktu and Cairo were taken from TRNSYS@ software. For consistency, the same sink temperature is considered for all climates even though Timbuktu and Cairo are not near the Red Sea, as the aim of this study is to compare different climates and not the specific cities.

The structure of this paper is as follows: first, the concept design of the closed air recirculation greenhouse coupled with a multi-stage NF regenerator is explained. Next, equations are provided to model the regenerator and to calculate the greenhouse temperature and relative humidity. Then, the greenhouse temperature results are plotted for different operating conditions and locations, showing the improvement relative to conventional greenhouse cooling methods. The monthly *COP* of the system and the monthly power requirement of the regenerator are also presented. The main design parameters are varied to give a better understanding of the system. Finally, the results and future improvements of the proposed multi-stage NF regenerator are discussed.

2. Concept

The design of the closed recirculation LDAC greenhouse is shown in Fig. 1. Unlike in the open ventilated greenhouse proposed earlier [1,41,42], the evaporative cooling pad is no longer used for three reasons. Firstly, evaporative cooling requires large amounts of water [9,43], which might be unavailable in many locations of interest. Secondly, closed recirculation can attain low indoor temperatures without the need of an evaporative cooling pad. Thirdly, an evaporative cooling pad would risk increasing the *RH* above 90 %, which is the maximum recommended for greenhouse crops [5]. Without the evaporative cooling pad, however, there is a risk of overheating at the early stages of cultivation when the crops are small and transpire less – such that the *RH* may decrease below 70 % which is the minimum recommended for typical crops [5]. Since transpiration assists cooling by converting sensible into latent heat, such decreased transpiration could lead to temperatures above 32 °C which is the maximum recommended for typical crops. Nonetheless, this risk could be addressed by using additional shading during early-stage cultivation, or by using misting to enhance cooling, such that evaporative cooling pads are avoided.

The dehumidifier can be a wetted pad (similar in construction to an evaporative cooling pad), with LD flowing over it, absorbing moisture and heat from the incoming air. The cooled and dehumidified air is then sent to the crops. Inside the greenhouse, the air temperature and the absolute humidity increase. The temperature increases due to the solar radiation and heat transferred through the cladding, while the absolute humidity increases due to crop transpiration. The hot and humid air leaving the crops is recirculated to the input of the dehumidifier.

As the LD passes through the dehumidifier, its temperature increases. The LD can be cooled using seawater from the Red Sea near Mecca which has a maximum temperature of 30 °C during the year, meaning it is

[1] Units in brackets are used in this study while units in braces are the equivalent SI units. Litres, bars, and hours are commonly used in membrane applications.

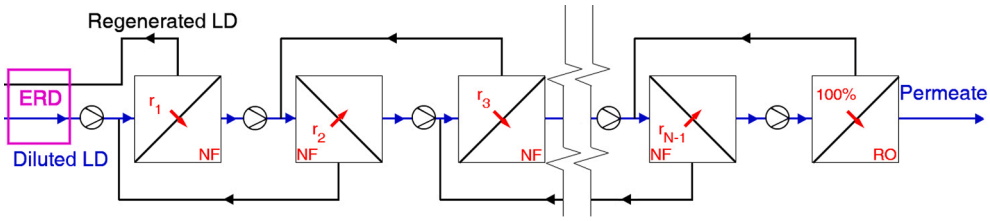

Fig. 2. Schematic of a N-stage nanofiltration (NF) regenerator. The diluted liquid desiccant (LD) enters the system while the outputs are the regenerated LD and the permeate. The system is composed of N-1 NF membranes with rejections r_i, where "i" indicates the positioning number of the membrane. The last membrane is a reverse osmosis (RO) with a rejection of ~ 100%. The NF membranes have rejections in the range of 10–50%. The system includes an energy recovery device (ERD) that decreases the energy consumption of the system. A pump is placed before every membrane which pressurises the feed to the desired pressure. In industrial applications, NF membranes operate at ~ 40 bar while RO membranes at ~ 70 bar.

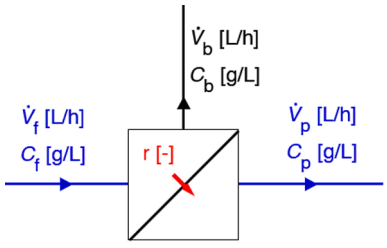

Fig. 3. Schematic of a generic membrane. The "$\dot{V}$" values represent flowrates [L/h], "C" concentrations [g/L] and "r" the rejection of the membrane [–]. The subscript letter "f" represents the feed, "b" represents the brine and "p" the permeate of the membrane.

possible to cool the LD to 30 °C year-round.

As the LD absorbs moisture from the air, it becomes diluted and needs to be regenerated. Fig. 2 shows the proposed NF regenerator consisting of multiple membrane stages. The first stage receives as input LD from the dehumidifier. Every stage has two outputs, i.e., the permeate (which is more diluted than the feed) and the brine (which is more concentrated than the feed). Every stage has a specific rejection (r) which is in the range of 10–50 % for commercial NF membranes [4,44–48]. Therefore, the permeate from each stage contains a certain amount of LD. Due to the high concentration of the LD, as required for efficient dehumidification, the osmotic pressure difference is higher than the burst pressure of the membrane. Therefore, membranes with high rejection cannot produce any permeate. For this reason, the first NF membrane must have a low rejection. The input LD entering the following stage is less concentrated, and thus, the rejection can be higher than in the previous stage. The NF membranes should be arranged with increasing rejections until the permeate is sufficiently diluted to operate with nearly 100 % rejection (RO membrane). The brine of the first stage is the regenerated LD, while the brine of each subsequent stage must be recirculated to the input of the respective upstream stage to avoid desiccant losses. The final stage is a RO membrane which produces pure water; its flowrate should be equal to the moisture that the LD absorbed in the dehumidifier. Therefore, the NF rejections should also be adjusted based on the absorbed moisture. Moreover, the permeate from the multi-stage system may be used for irrigation, thus closing the water cycle by returning the transpired water to the crops.

The multi-stage regenerator requires power for the pump upstream of each stage. The power requirement is approximately proportional to the number of stages, but not exactly. Due to the high osmotic pressure difference, a small number of stages may not be able to regenerate concentrated LDs. Many stages can regenerate highly concentrated LDs, but if there are too many stages, the power requirement increases with little benefit. Therefore, an optimal number of stages must exist that minimises the power requirement for a given LD concentration. As a rule, the rejections of the NF membranes should be as high as possible based on the concentration of the feed but should also be chosen based on the target moisture removal rate.

The power requirement can be decreased by using an energy recovery device (ERD) to capture the high pressure of the outlet brine and transfer its energy to the input feed, thus avoiding wastage of this energy [49]. The proposed system has PV collectors on top of the greenhouse to generate electricity to power the multi-stage regenerator. The PV panels also provide shading which reduces the heat load entering the greenhouse. However, the shading factor should not be too high, otherwise photosynthesis would be slowed down.

3. Modelling

The model of the system includes: the multi-stage NF regenerator, the dehumidifier, and the greenhouse. The modelling of the NF regenerator is developed first at the level of a single membrane stage, then at the level of the multi-stage system by considering mass and flow balances among the stages. Following the approach of Wang et al. [31], this study assumes that the pressure applied to each membrane equals the osmotic pressure difference across it. However, unlike in Wang et al., the osmotic pressure difference is calculated using the Gibbs energy and not the Van't Hoff equation which is an approximation valid only for dilute solutions. Since the LD must be highly concentrated in LDAC applications, such an approximation would be invalid for this study. Also, in contrast to Wang et al., the proposed design uses the RO membrane in the last rather than the first stage. Due to the high concentration of the LD, a RO membrane in the first stage would not produce any permeate since the osmotic pressure difference would be higher than the applied pressure. Therefore, a low rejection NF membrane is required at the first stage of the multi-stage system, with gradually increasing rejections in subsequent stages.

Then, a dehumidifier model is used to calculate the output conditions of the air and the LD passing through the dehumidifier. This model is based on the vapour pressure difference which is the driving force of the absorption rate. The dehumidifier is modelled using an iterative method which calculates how much moisture must be absorbed by the LD to equilibrate the vapour pressures, while also accounting for energy balance. The modelling of the dehumidifier is presented in detail in Appendix B. Finally, the greenhouse is modelled by accounting for the solar radiation, the effect of the ambient conditions and the crop transpiration.

The three models, though not validated directly in this study, have been validated elsewhere. The multi-stage NF regenerator is based on the seminal work of Wang et al. [31] and is based on mass and flow conservation equations and thermodynamic principles. We have developed this work further, by adding the Gibbs energy equation to calculate the osmotic pressure more accurately at high concentrations. The greenhouse model is similar to Davies' model [1] which was experimentally validated by Abu-Hamdeh and Almitani [41] who investigated a 300 m^2 in Saudi Arabia and found errors < 6 % using air mass flows of 3–30 kg/s. Our greenhouse model also includes a refinement in the calculation of crop transpiration, by making use of the model of Stanghellini [50]. Although there are different models of crop transpiration, comparative experimental studies found the Stanghellini model to be the

most accurate for use in greenhouses [51,52].

3.1. Modelling of the multi-stage regenerator

A schematic of a generic membrane with the input and outputs is shown in Fig. 3. Each membrane must satisfy the flow and mass conservation equations and the equation of the rejection (r). Regarding the flow conservation, the feed flowrate entering a membrane ($\dot{V}_f$) [L/h] must be equal to the sum of the output flowrates of the brine ($\dot{V}_b$) [L/h] and the permeate ($\dot{V}_p$) [L/h], as described in Eq. (1).

$$\dot{V}_f = \dot{V}_b + \dot{V}_p \tag{1}$$

Regarding the mass conservation, the product of the feed concentration (C_f) [g/L] and feed flowrate must be equal to the product of the brine concentration (C_b) [g/L] and brine flowrate plus the product of the permeate concentration (C_p) [g/L] and permeate flowrate, as described in Eq. (2).

$$\dot{V}_f C_f = \dot{V}_b C_b + \dot{V}_p C_p \tag{2}$$

Lastly, the rejection (r) [–] is defined as:

$$r = 1 - \frac{C_p}{C_f} \tag{3}$$

The osmotic pressure difference ($\Delta\Pi$) based on Gibbs energy [bar] can be calculated as (adapted from [53]):

$$\Delta\Pi = \frac{T_K R\left[\ln(\alpha_{w,p}) - \ln(\alpha_{w,b})\right]}{V'} \tag{4}$$

where $\Delta\Pi$ is assumed equal to is the applied pressure (ΔP) [bar], $R = 0.0832\,\mathrm{L\,bar/(K\,mol)}$ is the universal gas constant, T_K is the temperature [K], $V' = 0.018\,\mathrm{L/mol}$ is the inverse of the pure water molarity, $\alpha_{w,p}$ and $\alpha_{w,b}$ are the water activities of the permeate and brine [–], respectively. The water activity depends on the concentration of the LD. Conde et al. [54] reported the water activity (α_w) of $CaCl_2$ for various concentrations; these data were used to create a polynomial fit of the water activity as function of concentration:

$$\alpha_{w,CaCl2} = 26.96x^4 - 19.23x^3 + 0.6232x^2 - 0.4079x + 1 \tag{5}$$

where x is the $CaCl_2$ mass fraction per mass of solution [–]. The outputs of a membrane can be calculated by rearranging Eq. (1), (2), (3) and (4). The concentration of the permeate of the membrane can thus be calculated as:

$$C_p = C_f(1 - r) \tag{6}$$

The water activity of the brine can be calculated as:

$$\alpha_{w,b} = \exp\left[\ln(\alpha_{w,p}) - \frac{\Delta P \times V'}{T_K R}\right] \tag{7}$$

where the concentration of the brine (wt_b) [wt.%] can be calculated using Eq. (5) as:

$$wt_b = -498{\alpha_{w,b}}^4 + 1091{\alpha_{w,b}}^3 - 853.6{\alpha_{w,b}}^2 + 236\alpha_{w,b} + 25.46 \tag{8}$$

wt_b is converted to C_b [g/L] using the following equation:

$$C_b = \frac{\frac{wt_b}{10^2 - wt_b}}{10^{-3} + \frac{wt_b/\rho_{CaCl2}}{10^2 - wt_b}} \tag{9}$$

where ρ_{CaCl2} is the density of pure $CaCl_2$ equal to 2150 kg/m^3. The output flowrates of the membrane are calculated by rearranging Eqs. (1) and (2), thus:

$$\dot{V}_b = \dot{V}_f \frac{C_f - C_p}{C_b - C_p} \tag{10}$$

$$\dot{V}_p = \dot{V}_f - \dot{V}_b \tag{11}$$

In a multi-stage NF system, the inputs and outputs of the membranes are related to each other. For a N-stage system composed of N-1 NF membranes and a last RO membrane, the feed flowrate of the j^{th} NF membrane ($\dot{V}_{f,j}$) [L/h] is equal to the sum of the permeate flowrate of the previous membrane ($\dot{V}_{p,j-1}$) [L/h] and the brine flowrate of the next membrane ($\dot{V}_{b,j+1}$) [L/h], as described by Eq. (12). For an N-stage system, j is between 1 and N-1.

$$\dot{V}_{f,j} = \dot{V}_{p,j-1} + \dot{V}_{b,j+1} \tag{12}$$

Similarly, the feed concentration of the j^{th} NF membrane ($C_{f,j}$) [g/L] is given by:

$$C_{f,j} = \frac{\dot{V}_{p,j-1}C_{p,j-1} + \dot{V}_{b,j+1}C_{b,j+1}}{\dot{V}_{f,j}} \tag{13}$$

Since there is no brine recirculation in the last RO membrane (j = N), the feed flowrate ($\dot{V}_{f,N}$) [L/h] and concentration ($C_{f,N}$) [g/L] at the RO membrane are given by:

$$\dot{V}_{f,N} = \dot{V}_{p,N-1} \tag{14}$$

$$C_{f,N} = \frac{\dot{V}_{p,N-1}C_{p,N-1}}{\dot{V}_{f,N}} \tag{15}$$

The electric power requirement of the N-stage NF system (P_{system}) [kW] is given by the sum of the power requirements of the pumps ($P_{pump,j}$) [kW] preceding each membrane (j is between 1 and N). The power consumption of each pump is calculated as:

$$P_{pump,j} = \frac{\Delta P \times \dot{V}_{p,j-1}}{36 \times 10^3 \eta_{pump}} \tag{16}$$

where $P_{pump,j}$ is the power requirement of the pump before the j^{th} membrane [kW], $\dot{V}_{p,N-1}$ is the fluid flowrate [L/h] entering the pump before the jth membrane. For the first membrane (j = 1), $\dot{V}_{p,0}$ is equal to $\dot{V}_{f,1}$. η_{pump} is the standard overall efficiency of the pump, assumed equal to 0.85 based on manufacturer datasheets [55]. ΔP is set to 40 bar for the NF membrane [44–47] and 70 bar for the RO membrane [24]. An ERD can be used to save energy (P_{ERD}) [kW] that would be wasted otherwise, calculated as:

$$P_{ERD} = \frac{\Delta P \times \dot{V}_{b,1}\eta_{ERD}}{36 \times 10^3} \tag{17}$$

where η_{ERD} is the efficiency of the ERD, assumed equal to 0.9. Therefore, P_{system} is calculated as:

$$P_{system} = \sum_{j=1}^{N} P_{pump,j} - P_{ERD} \tag{18}$$

The specific work of the multi-stage NF regenerator (W_{SP}) [kJ/kg] is given by dividing P_{system} with the permeate flowrate of the last stage ($\dot{V}_{p,end}$) [L/h]:

$$W_{SP} = 3600\frac{P_{system}}{\dot{V}_{p,end}} \tag{19}$$

For the main case study (LD mass flow of 20 kg/s, LD concentration of 15 wt% and LD temperature of 30 °C), it was found that the specific work of the multi-stage NF regenerator is 309.6 kJ/kg.

Due to the brine recirculation, the above equations initially indicate time-varying feed flowrates at each stage, which converge to steady values after a certain simulation time. Since a high number of stages is required for concentrated LDs, the system is complex and can be solved using software, such as MATLAB-Simulink®. For instance, $CaCl_2$ with a concentration of 15 wt% requires at least 9 stages. This concentration

Table 1
Values of constant parameters used for the greenhouse model, values with an "*" are taken from Davies [1].

Parameter	Value	Unit	Full name of parameter
α	0.7*		Absorbance of greenhouse floor with crop
β	0.5*		Fraction of roof area covered by PV collectors
τ	0.8*		Roof transmittance
h	0.0042*	kW/(m^2 K)	Heat loss coefficient
A_{gh}	250*	m^2	Floor area of the greenhouse
A_s	450*	m^2	Surface area of the greenhouse
$\dot{m}_{Air}$	20	kg/s	Air mass flow
$c_{p,Air}$	1.013	kJ/(kg K)	Heat capacity of the air
LAI	0.8	m^2/m^2	Leaf area index
k_c	0.45		Crop coefficient
$\dot{m}_{LD}$	20	kg/s	Liquid desiccant mass flow
η_{PV}	0.18		Efficiency of the photovoltaic collectors
η_{pump}	0.85		Efficiency of the pump
ε_{evap}	0.8		Effectiveness of the evaporator

was used for the main case study because it allows the *RH* to remain in the optimal crop range of 70–90 %.

3.2. Modelling of the greenhouse

After the dehumidifier (explained in appendix B), the temperature in the greenhouse increases due to the solar radiation and the hot external conditions. The greenhouse temperature can be calculated using the heat balance equations provided by Davies [1]:

$$\dot{Q}_{gh} = \dot{m}_{Air}\, c_{p,Air}(T_{out} - T_{cool}) + hA_s(T_{gh} - T_{amb}) + ET_c\lambda \tag{20}$$

$$\dot{Q}_{gh} = IA_{gh}\tau\alpha(1-\beta) \tag{21}$$

$$T_{gh} = \frac{T_{cool} + T_{out}}{2} \tag{22}$$

where $\dot{Q}_{gh}$ is the exchanged heat in the greenhouse [kW], $\dot{m}_{Air}$ is the air mass flow [kg/s], $c_{p,Air}$ is the air heat capacity [kJ/(kg K)], h is the heat loss coefficient [kW/(m^2 K)], A_s is the greenhouse surface area [m^2],I is the solar radiation [kW/m^2], A_{gh} is the greenhouse flour area [m^2], τ is the roof transmittance [-], α is the absorbance of greenhouse floor with crop, β is the fraction of A_{gh} covered by PV collectors [-], ET_c is the crop transpiration rate [kg/s] and λ is the latent heat of evaporation [kJ/kg]. It is assumed that the temperature inside the greenhouse (T_{gh}) is equal to the average of the cool air sent to the crops (T_{cool}) and the air temperature at the end of the greenhouse (T_{out}).

The performance of the proposed closed recirculated LDAC system (*closed: fan+dess*) is compared with three conventional open ventilated cooling technologies: simple fan ventilation (*fan*), evaporative cooling using a fan to draw air through an evaporative cooling pad (*fan+evap*) and a system composed of a fan to draw air through a dehumidifier, a dehumidifier and an evaporative cooling pad (*fan+evap+dess*). For these four cooling technologies, T_{cool} is equal to:

(a) *fan*: $T_{cool} = T_{amb}$
(b) *fan+evap*: $T_{cool} = T_{amb} - \varepsilon_{evap}\left(T_{amb} - T_{wb}{}^{amb}\right)$
(c) *fan+evap+dess*: $T_{cool} = T_{out}{}^{deh} - \varepsilon_{evap}\left(T_{out}{}^{deh} - T_{wb}{}^{deh}\right)$
(d) *closed: fan+dess*: $T_{cool} = T_{out}{}^{deh}$

where $T_{wb}{}^{amb}$ is the wet-bulb temperature of the ambient air, ε_{evap} is the effectiveness of the evaporative cooling pad, $T_{out}{}^{deh}$ is the outlet air temperature from the dehumidifier and $T_{wb}{}^{deh}$ is the wet-bulb temperature of the air leaving the dehumidifier. $T_{out}{}^{deh}$ is calculated using Eqs. (B.1)-(B.14), as described in Appendix B.

The temperature parameters in Eqs. (20)–(22) can be seen in Fig. 1 for a better understanding. The combination of Eqs. (20)–(22), yields:

$$T_{gh} = \frac{IA_{gh}\tau\alpha(1-\beta) - ET_c\lambda + 2\dot{m}_{Air}c_{p,Air}T_{cool} + hA_sT_{amb}}{2\dot{m}_{Air}c_{p,Air} + hA_s} \tag{23}$$

$$T_{out} = 2T_{gh} - T_{cool} \tag{24}$$

Since the model assumes closed recirculation, it is necessary to calculate the humidity ratio (ω) increment resulting from the crop transpiration (ET_c). ET_c [kg/s] is calculated as [50]:

$$ET_c = \frac{2k_cLAI}{\lambda}\frac{\frac{\Delta\times R_n}{3600} + \frac{\left(VPD\rho_{Air}c_{p,Air}\right)}{r_R}}{\Delta + 0.06735\left(1 + \frac{r_c}{r_a}\right)}A_{gh} \tag{25}$$

where k_c is the crop coefficient [–], LAI is the leaf area index [m^2/m^2], Δ is the slope of the saturation vapour pressure curve [kPa/K], R_n is the net radiation above the canopy [kJ/(m^2 h)], VPD is the vapour pressure deficit of the air [kPa], ρ_{Air} is the density of the air [kg/m^3], r_R is the radiative resistance [s/m], r_c is the internal resistance of the canopy [s/m] and r_a is the aerodynamic external resistance [s/m]. The equations to calculate these parameters are given in Appendix A. The humidity ratio at the exit of the greenhouse (ω_{out}) [g_v/kg_a] can be calculated as:

$$\omega_{out} = 10^3\frac{\dot{m}_{v,cool} + ET_c}{\dot{m}_{d,cool}} \tag{26}$$

where $\dot{m}_{v,cool}$ is the moisture mass flow at the exit of the dehumidifier [kg/s] and $\dot{m}_{d,cool}$ is the mass flow of dried air at the exit of the dehumidifier [kg/s][2]. Having calculated T_{out} and ω_{out}, the air conditions at the end of the greenhouse are fully determined. This air is recirculated to the dehumidifier.

Generally, the *COP* is calculated as the heating or cooling power output divided by the required input power [56]. In this case, the *COP* is calculated as the produced cooling power divided the electric power requirement of the multi-stage NF regenerator P_{system} [kW]:

$$COP = \frac{\dot{Q}_{gh}}{P_{system}} \tag{27}$$

where P_{system} is the electric power requirement of the multistage NF system[kW].

The multi-stage regenerator is assumed to be powered by PV collectors with power output P_{PV} [kW] given by:

$$P_{PV} = \eta_{PV}I\beta A_{gh} \tag{28}$$

where η_{PV} is the efficiency of the PV collectors, assumed equal to 18 % based on commercial PV collectors [57]. The P_{PV} values in the Results section are calculated using maximum solar radiations. Since the solar radiation varies based on time and climatic conditions, it is assumed that the PV collectors also include a solar battery storage. Thus, the multi-stage NF regenerator absorbs the required power from the solar battery storage when the power is needed.

Eqs. (20)–(27) are used in an iterative method to simulate the closed recirculation of the greenhouse. The model presented in this study is steady state, corresponding to 7 iterations as required for the convergence of T_{gh} (percentage difference from the 6th iteration is 0.02 %).

Due to their high thermal inertia, residential buildings usually require dynamic models for accurate predictions. For greenhouses, however, steady-state models are often sufficient as shown in previous studies. For example, Kittas et al. [42] investigated a commercial greenhouse with an evaporative cooling system and found good agreement between their steady-state model and experimental results. The authors measured the temperature at the middle of the greenhouse with an error of 6 % compared to their model. They also measured the

[2] The sum of $\dot{m}_{v,cool}$ and $\dot{m}_{d,cool}$ is equal to $\dot{m}_{Air}$.

Table 2
Maximum monthly solar radiations, maximum monthly ambient temperatures and average monthly ambient relative humidities for a) Mecca (*hot and humid*), b) Timbuktu (*hot and arid*) and c) Cairo (*semi-hot and semi-arid*) taken from TRNSYS® software.

	Maximum ambient temperature [°C]											
a	34.7	35.15	39.05	41.2	44.75	45.45	46.35	44	43.9	41.4	37.3	34.85
b	33.1	36.05	38.65	41.55	42.6	42.25	42.35	38.85	39.65	39.3	35.3	31.6
c	22.4	25.65	31.15	36.5	37.5	38.65	39.15	35.9	36.3	33.15	28.5	23.95
	Maximum solar radiation [kW/m^2]											
a	0.820	0.953	1.004	1.039	1.053	1.057	1.054	1.027	1.012	0.993	0.890	0.787
b	0.843	0.940	0.995	1.000	0.997	0.970	0.973	0.976	0.968	0.933	0.866	0.820
c	0.658	0.786	0.909	0.976	0.988	1.010	0.989	0.951	0.906	0.822	0.695	0.593
	Average ambient relative humidity [%]											
a	77.5	78.5	72	64	63	59	62	70.5	74	74.5	81	89
b	33.16	25.85	26.42	34.93	42.36	49.65	56.24	68.03	65.91	55.66	38.17	36.14
c	59.4	52.57	49.74	43.63	41.62	46.54	55.25	58.85	58.58	56.96	61.08	62.59

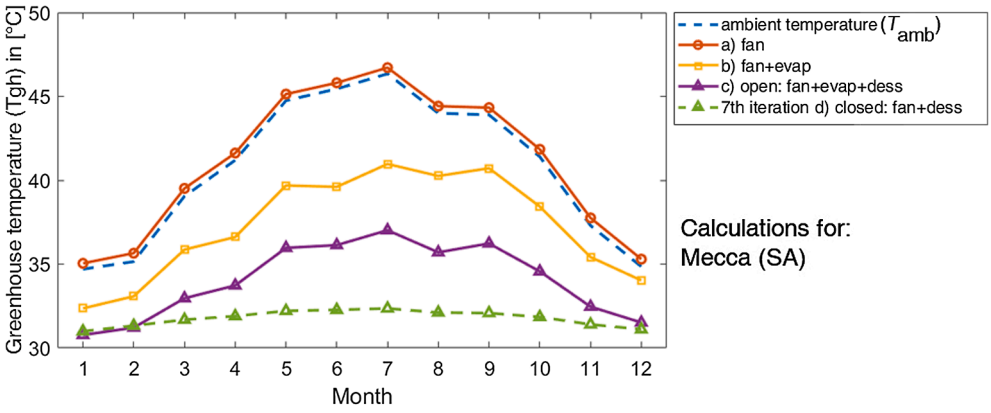

Fig. 4. Monthly ambient temperatures (T_{amb}) and monthly greenhouse temperatures (T_{gh}) calculated for four cooling configurations. a) simple fan ventilation (fan); b) conventional evaporative cooling using a fan (to draw air through an evaporative cooling pad) and an evaporative cooling pad (*fan+evap*), c) system composed of a fan (to draw air through a dehumidifier), a dehumidifier and an evaporative cooling pad (*fan+evap+dess*) and d) the proposed system with only a dehumidifier and a multi-stage nanofiltration regenerator (*closed: fan+dess*). Cases a, b and c are illustrated in a previous paper [1]. Case d) shows the results for the seventh (last and convergent) model iteration. Case d) is illustrated in Fig. 1. These results are regarding *hot and humid* climates (such as Mecca, Saudi Arabia).

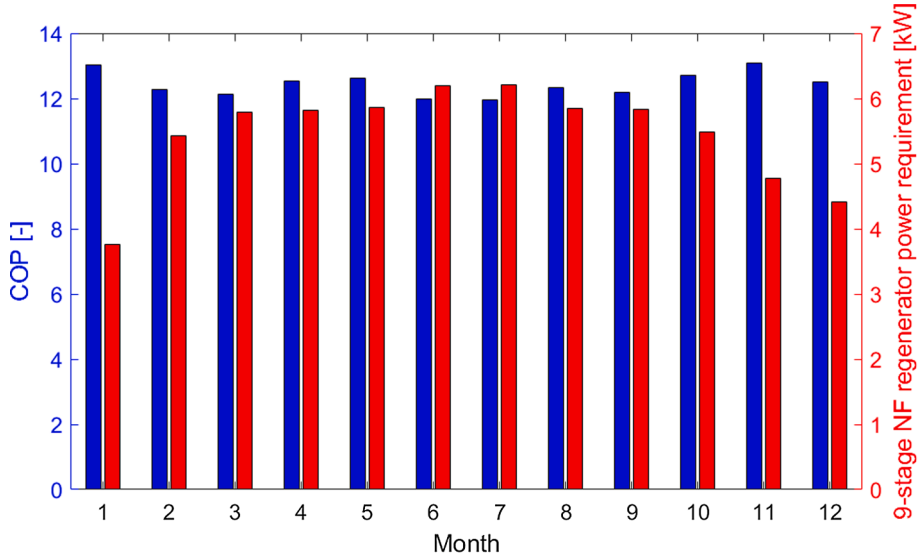

Fig. 5. Monthly coefficient of performance (*COP*) for the proposed system (*closed: fan+dess*) which uses a 9-stage nanofiltration (NF) regenerator (values on the left y-axis) and monthly power requirement of the 9-stage NF regenerator [kW$_{el}$] (values on the right y-axis). The results are regarding *hot and humid* climates (such as Mecca, Saudi Arabia) for a 250 m^2 greenhouse.

temperature at the end of the greenhouse with an error of 3 % compared to their model. More recently, Abu-Hamdeh and Almitani [41] experimentally investigated a 300 m^2 greenhouse and compared their results using the steady-state model of Davies' study [1] (our paper is also based on Davies' study). The authors measured the greenhouse temperature with air mass flows of 3–30 kg/s for a conventional evaporative cooling system and a desiccant cooling system and found the steady-state model to be accurate (error < 6 %). Steady-state models give reliable results for greenhouses because greenhouses have lighter structures and higher air changes than residential buildings, making thermal inertia less

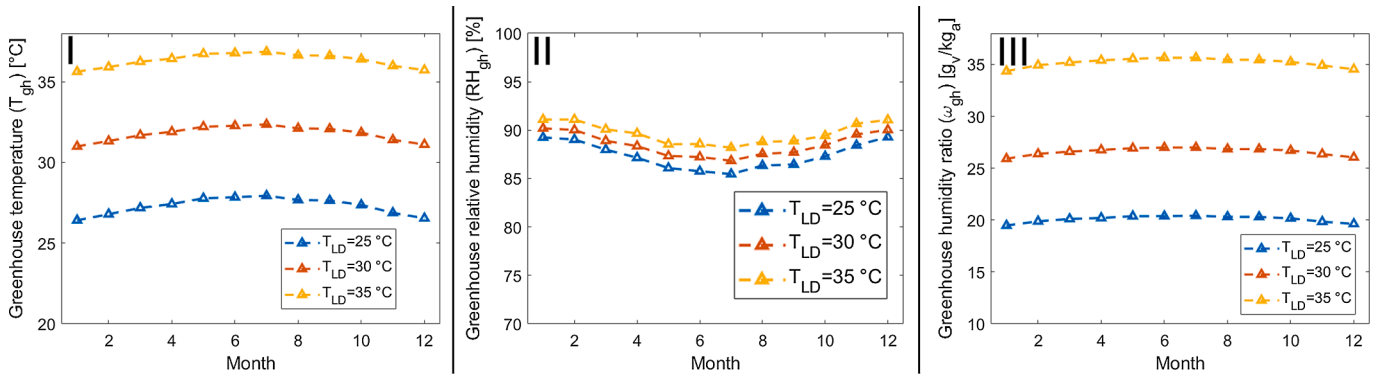

Fig. 6. I) Monthly greenhouse temperatures (T_{gh}) [°C], II) monthly greenhouse relative humidities (RH_{gh}) [%], and III) monthly greenhouse humidity ratios (ω_{gh}) [g_v/kg_a] considering: LD temperatures (T_{LD}) of 25, 30 and 35 °C. These results are regarding *hot and humid* climates (such as Mecca, Saudi Arabia) for the proposed system (*closed: fan+dess*).

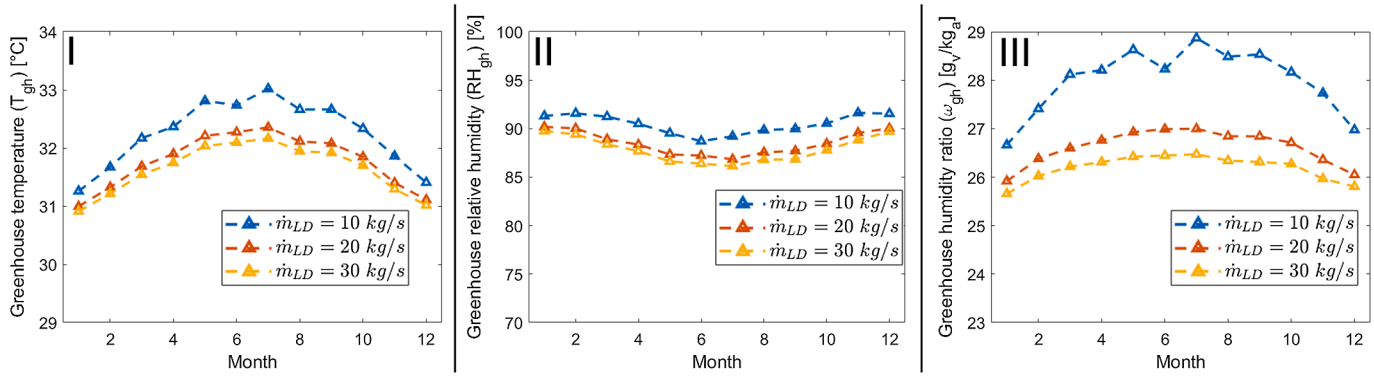

Fig. 7. I) Monthly greenhouse temperatures (T_{gh}) [°C], II) monthly greenhouse relative humidities (RH_{gh}) [%], and III) monthly greenhouse humidity ratios (ω_{gh}) [g_v/kg_a] considering: LD mass flows ($\dot{m}_{LD}$) of 10, 20 and 30 kg/s. These results are regarding *hot and humid* climates (such as Mecca, Saudi Arabia) for the proposed system (*closed: fan+dess*).

Table 3
Results for the electric power requirement of the 9-stage NF regenerator (P_{system}) [kW_{el}] and the specific work (W_{SP}) [kJ/kg] considering LD mass flows of 10, 20 and 30 kg/s.

$\dot{m}_{LD}$ [kg/s]	P_{system} [kW_{el}]	W_{SP} [kJ/kg]
10	7.051	378.9
20	6.212	309.6
30	5.334	281.8

important.

The values of the constant parameters used in this study are summarised in Table 1. The values regarding the greenhouse dimensions and materials are based on typical greenhouses, taken from Davies [1]. The values for the maximum monthly solar radiations, maximum monthly ambient temperatures and average monthly ambient relative humidities for Mecca (*hot and humid*), Timbuktu (*hot and arid*) and Cairo (*semi-hot and semi-arid*) are shown in Table 2. The weather data was taken from TRNSYS® software (which generates the weather data using Meteonorm version 5.0.13).

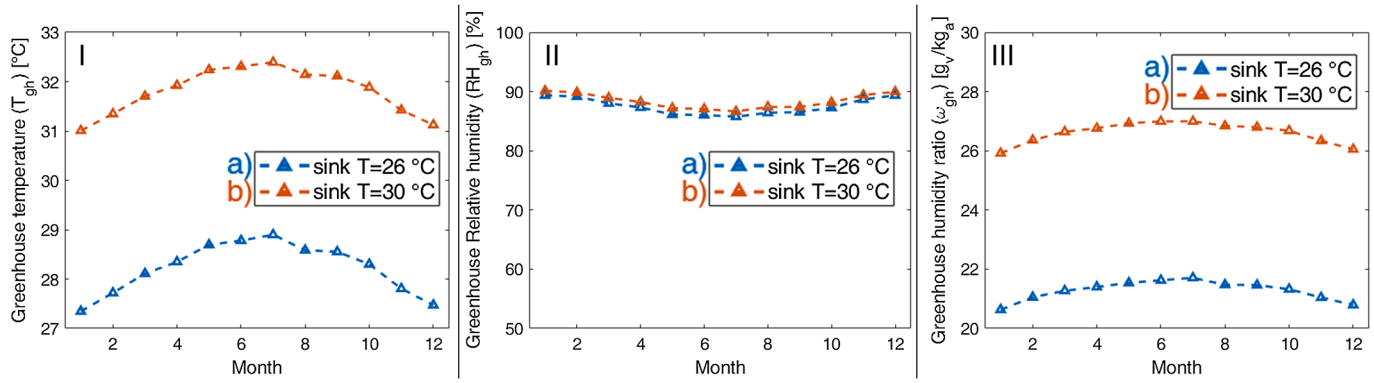

Fig. 8. I) Monthly greenhouse temperatures (T_{gh}) [°C], II) monthly greenhouse relative humidities (RH_{gh}) [%], and III) monthly greenhouse humidity ratios (ω_{gh}) [g_v/kg_a] considering: sink temperatures (*sink T*) of 30 and 26 °C. These results are regarding *hot and humid* climates (such as Mecca, Saudi Arabia) for the proposed system (*closed: fan+dess*).

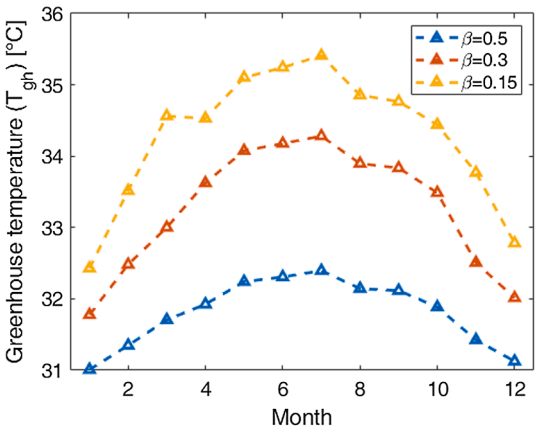

Fig. 9. Monthly greenhouse temperatures (T_{gh}) [°C] calculated for fractions of roof area covered by PV collectors (β) of 0.5, 0.3 and 0.15. These results are regarding *hot and humid* climates (such as Mecca, Saudi Arabia) for the proposed system (*closed: fan+dess*).

4. Results

The monthly greenhouse internal temperatures (T_{gh}) were calculated using the equations shown in the Modelling section (Fig. 4). T_{gh} is different for the four technologies, namely *fan, fan+evap, fan+evap+dess* and *closed: fan+dess*, corresponding to differing equations to calculate T_{cool}. These results were calculated using maximum solar radiations, maximum ambient temperatures and average relative humidities for *hot and humid* conditions (such as Mecca, Saudi Arabia). For *closed: fan+dess,* Fig. 4 includes results for the seventh (i.e. final and convergent) model iteration.

Regarding the *COP*, this remains between 11.9 and 13, with an average of 12.4 during the year (Fig. 5). The *COP* depends on the power requirement of the 9-stage NF regenerator (P_{NF}), which has a maximum of 6.212 kW (Fig. 5). The *COP* is calculated using maximum solar radiations which represent the worst conditions for the greenhouse. On the other hand, maximum solar radiations allow the PV collectors to produce the achievable power.

The results of Figs. 4 and 5 were calculated for the main case study which uses $CaCl_2$ with a mass flow of 20 kg/s, concentration of 15 wt% and temperature of 30 °C. The LD temperature is an important parameter that can affect the greenhouse conditions. Therefore, three LD temperatures of 25, 30 and 35 °C have been considered and the results for the monthly T_{gh}, RH_{gh} and ω_{gh} are shown in Fig. 6.

Other parameters with a significant effect are the LD mass flow, the sink temperature and the fraction of roof area covered by PV collectors (β). Regarding the LD mass flow, the monthly T_{gh}, RH_{gh} and ω_{gh} are shown in Fig. 7 for LD mass flows of 10, 20 and 30 kg/s.

Lower T_{gh} and RH_{gh} can be achieved with higher LD mass flows, but T_{gh} and RH_{gh} change marginally between LD mass flows of 20 and 30 kg/s. Since a LD mass flow of 30 kg/s would be hard to achieve at the dehumidifier, the LD mass flow of the main case study was therefore set to 20 kg/s. The results for the three investigated LD mass flows regarding the electric power requirement of the 9-stage NF regenerator (P_{system}) [kW_{el}] and the specific work (W_{SP}) [kJ/kg] are summarised in Table 3.

Regarding the sink temperature, this study considers a sink temperature of 30 °C which is the maximum temperature of the red sea near Mecca. The sink temperature is important as lower sink temperatures allows lower T_{gh}. Fig. 8 shows the results for the monthly T_{gh}, RH_{gh} and ω_{gh} having sink temperatures of 30 and 26 °C. The sink temperature of 26 °C is arbitrary and was selected as a temperature below 30 °C to compare with the sink temperature of 30 °C.

Regarding the effect of β, this study considered a β of 0.5, but the theoretical ideal minimum β for single-band gap PV collectors would be 0.15 [58]. The T_{gh} increases by 3 °C by decreasing β from 0.5 to 0.15 (Fig. 9). Since β of 0.5 can maintain the T_{gh} below 32 °C (maximum allowable), β of 0.5 was selected for this study.

Finally, the effect of the climate is also investigated. The main case study climate is *hot and humid* (like Mecca, Saudi Arabia), but the same greenhouse model was evaluated for *hot and arid* (like Timbuktu, Mali) and *semi-hot and semi-arid* climates (like Cairo, Egypt). Fig. 10 shows the monthly T_{gh} for these other two climate types.

5. Discussion

In *hot and humid* climates, such as Mecca, the technology using only a fan (*fan*) does not provide any cooling; thus T_{gh} is equal to the ambient temperature. The addition of an evaporative cooling pad (*fan+evap*) achieves a temperature drop of ~ 5.8 °C compared to the *fan* only during summer; while the addition of both an evaporative cooling pad and a dehumidifier (*fan+evap+dess*) achieves a temperature drop of ~ 8.9 °C compared to the first option (*fan*) during summer (Fig. 4). The proposed LDAC system, operating in closed recirculation with only a dehumidifier (*closed: fan+dess),* can attain even lower temperatures, having T_{gh} ~ 4 °C lower than the *fan+evap+dess* technology during summer.

The system was evaluated under variation of different parameters, including LD properties, sink temperature, and fraction of greenhouse shaded by PV collectors (β). Regarding the LD temperature, LD temperatures of 25, 30 and 35 °C were considered. Lower LD temperatures are preferred because they allow lower T_{gh} and RH_{gh} to be attained (Fig. 6). The LD mass flow was also investigated, with higher LD mass flows attaining lower T_{gh} and lower RH_{gh} (Fig. 7). If the rejections of the membranes were held constant, higher LD mass flow would result in

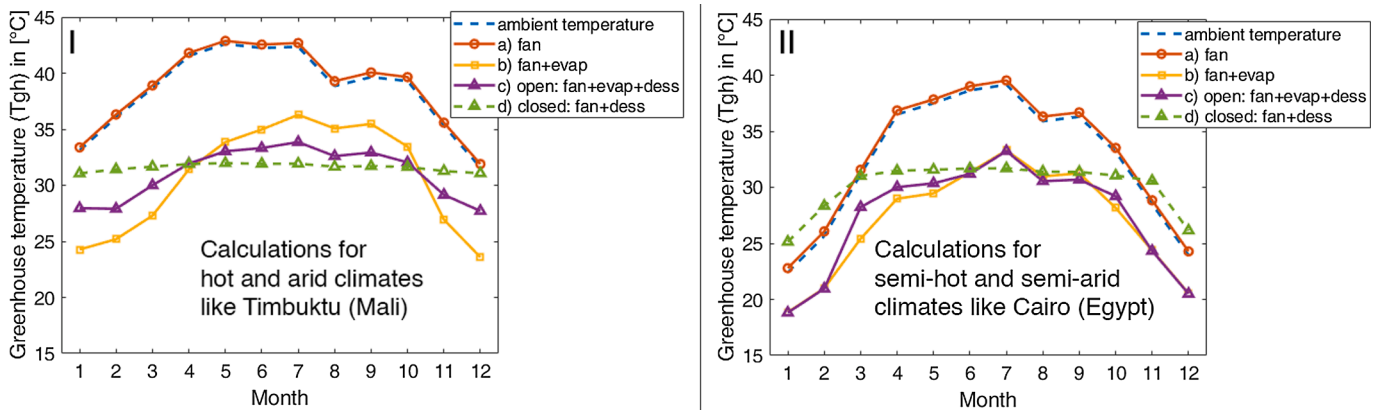

Fig. 10. Monthly ambient temperatures and monthly greenhouse temperatures (T_{gh}) calculated for four cooling configurations, as labelled in Fig. 4, considering weather conditions of I) *hot and arid* climate (like Timbuktu, Mali) and II) *semi-hot and semi-arid* climate (like Cairo, Egypt).

higher power requirement for the multi-stage NF system, because the power of the pumps is proportional to the mass flow. In practice, however, higher LD mass flow would require higher membrane rejections (to maintain the same overall moisture removal rate) which would decrease the flow recirculation rates of the multi-stage system, and thus decrease the power requirement of each pump. Consequently, higher LD mass flow decreases the electric power requirement and the specific work of the NF regenerator (Table 3).

Regarding the efficiency of the system for the main case study ($CaCl_2$ with a mass flux of 20 kg/s, a temperature of 30 °C and a concentration of 15 wt%), this reached an average *COP* of ~ 12.4 (Fig. 5), T_{gh} below $32^{\circ}C$, and RH_{gh} 90% during the year. This value approaches the ideal maximum of 14.33 according to Lefers et al. [9]. A *COP* of 12.4 is significantly higher than the experimentally obtained with open evaporative solar regenerators, where values of only 0.3–0.5 were reported [46]. Moreover, commercial chillers using vapour compression have *COP* values between 2.5 and 4.3, depending on the design category [59–61]. This means the proposed system using a multi-stage NF regenerator could allow *COP* values three times higher than these commercial technologies.

Though a 9-stage NF system may be complex and expensive, there is potential to reduce the number of stages with more robust NF membranes. The 9-stage system using an applied pressure of 40 bar for the NF membranes would require at most 6.212 kW to regenerate $CaCl_2$ with a concentration of 15 wt%, achieving a specific work of 309.6 kJ/kg. If the NF membranes could withstand a pressure of 55 bar, then a 4-stage regenerator would require at most 6.274 kW, with a specific work of 312.6 kJ/kg, while maintaining the same *COP* as the 9-stage regenerator. A burst pressure of 55 bar is reasonable since commercial RO membranes have burst pressures of 83 bar [28,29]. Thus, research regarding the fabrication of NF membranes with higher burst pressures could decrease the number of stages, the cost and the size of the regenerator. The reason the 4-stage regenerator would require slightly more power than the 9-stage regenerator is because the 4-stage regenerator could operate with higher rejections, resulting in an overall circulated flowrate slightly higher than in the 9-stage regenerator.

Regarding the effect of the sink temperature, this study considered a sink temperature of 30 °C (maximum Red Sea temperature during the year), but lower sink temperatures would result in lower T_{gh} (Fig. 8). A sink temperature of 26 °C could obtain T_{gh} of 3.6 °C lower than the sink temperature of 30 °C.

Regarding the effect of β, this study considered a β of 0.5 with a PV efficiency of 18 %. For $\beta = 0.5$, the PV collectors produce from 15.7 to 23.6 kW considering monthly maximum solar radiations. Since the maximum power of the multi-stage NF regenerator is only 6.212 kW (Fig. 5), the PV collectors can produce more power than required by the multi-stage regenerator. However, lower β results in T_{gh} above the allowed maximum of $32^{\circ}C$ because of lack of shading(Fig. 9), so this oversized PV collector is preferred. Excess electricity can be exported to the grid or stored in batteries for local use; for example, it may be helpful in maintaining system operation under transient conditions such as passing clouds. Another option is to use a lower PV collector area together with passive shading to achieve 50 % of overall shading and thus maintain the greenhouse temperature $<32^{\circ}C$.

Theoretically, β=0.15 is the minimum for ideal single-band gap PV collectors [58]. Although β of this study is higher than the ideal, future improvements in PV technology, such as higher PV efficiencies (η_{PV}) or selective PV cells, could lower β to values close to this ideal. Higher η_{PV} would capture the same solar energy with a smaller PV area, while selective PV cells that reject the infrared radiation would provide a lower greenhouse temperature. The infrared radiation makes up half of the total incoming radiation but, since infrared radiation is rejected by the crops [5], it only increases the greenhouse temperature. Therefore, selective PV cells would be a major improvement for greenhouse applications.

Based on the second law of thermodynamics, a regeneration system driven by a generic solar thermal collector could provide cooling with $\beta = 0.367$ [58]. However, experimental studies regarding open-type solar LD regenerators found that β up to 4 is required depending on the climate [12]. Closed-type solar LD regenerators have also been investigated for LD regeneration and are expected to be more energy efficient [62]. For example, Yang and Wang [63] investigated a closed-type solar collector coupled with an evaporator to regenerate a concentrated LiCl solution. Although their study did not calculate β (as they did not investigate greenhouses), a comparison can be made based on the evaporated water, which was 2.7 times higher than the open-type solar LD regenerator mentioned earlier [12]. Thus, closed-type solar LD regenerators could require a β of ~ 1.5 (but would also require water for the evaporator), which is still much higher than the value calculated for the NF regenerator. Therefore, this study shows that a multi-stage NF regenerator makes the system more compact, as the required β is several times lower compared to conventional solar regenerators using both open and closed collectors.

The effect of climatic conditions is mitigated by the greenhouse closed air recirculation. Thus, the system can maintain the monthly T_{gh} below 32 °C independently of the climate type (Fig. 10). During winter, in a *semi-hot and semi-arid* climate (such as Cairo), *fan+evap* and *fan+evap+dess* achieves lower T_{gh} than the proposed system (*closed: fan+dess*) during winter. This is because the T_{amb} is lower than the sink temperature (assumed equal to 30 °C). Therefore, the proposed LDAC system is advantageous when T_{amb} is above the sink temperature. During summer for *semi-hot and semi-arid* climates and during winter for the *hot and arid* climates (such as Timbuktu), *fan+evap* and *fan+evap+dess* attain lower temperatures than the proposed system (*closed: fan+dess*). This is because the evaporative cooling pad achieves low T_{gh} when operated with low RH_{amb}. Nonetheless, the evaporative cooling pad has high water demands. Based on energy balance equations in the evaporative cooling pad, 10.36 L of water evaporate daily during winter for every m^2 of greenhouse [L/(m^2 day)] (considering an inlet water temperature of 30 °C and an evaporative cooling pad effectiveness of 0.8). During summer, this value increases to 20.72 L/(m^2 day). Since the water supply must be higher than the rate of evaporation, the evaporative cooling pad would require at least 12 L/(m^2 day) of water during winter, and 24 L/(m^2 day) during summer. In practice, the flowrate would need to be even higher to avoid scaling and clogging of the evaporator pad (depending on the composition of the feed). Therefore, the proposed system could include an evaporative cooling pad and attain lower monthly T_{gh} for climates like Timbuktu and Cairo, but the water demand would be a problem for water-scarce locations.

A conventional greenhouse requires water for the evaporative cooling pad and for irrigation. The proposed LDAC design eliminates the need for the former because the LD is cooled using seawater (for example, using a liquid-to-liquid heat exchanger). Regarding the requirement for irrigation, this is typically close to the crop transpiration rate. LDAC also eliminates this requirement because the evaporated moisture from the crops is absorbed by the LD, collected as the permeate of the multi-stage NF regenerator, and used for irrigation. Consequently, the proposed system saves at least 16.8 L/(m^2 day) of water during winter, and 30.6 L/(m^2 day) during summer.

6. Conclusions

A novel LD regeneration system based on a multi-stage NF regenerator for a closed air recirculation greenhouse has been modelled. The novelty is the utilisation of NF membranes to remove the absorbed moisture from the LD in LDAC applications. This moisture can be recovered as the permeate of the multi-stage NF regenerator and used for irrigation. In contrast, open evaporative regenerators waste the moisture as they evaporate it to the atmosphere.

This study has evaluated the performance of the system considering

variable LD properties, sink temperatures, shading fraction β, and climate type. The results show that higher LD mass flow, higher β, lower LD temperature and lower sink temperature are better at maintaining the greenhouse in the optimal temperature range (27–29 °C [1]) and relative humidity range (70–90 % [5]) of typical greenhouse crops.

The proposed LDAC system is particularly advantageous in a *hot and humid* climate where the ambient temperature is above the sink temperature. For this type of climate, LDAC achieves temperatures of ~ 4 °C lower than conventional open ventilated cooling technologies during summer. Compared with technologies using evaporative cooling, the proposed system saves 16.8 L/(m^2 day) of water during winter, and 30.6 L/(m^2 day) during summer.

For *hot and arid* and *semi-hot and semi-arid* climates, the proposed system performs worse than the technologies using evaporative cooling. Nevertheless, it maintains the greenhouse temperature below 32 °C for all three investigated climate types. The proposed LDAC system does not include evaporative cooling, so it does not require a water supply. In contrast, evaporative cooling has the disadvantage that it can only operate in water-abundant locations.

For the main case study investigated here – which considers a 250 m^2 greenhouse using $CaCl_2$ as the LD with a mass flow of 20 kg/s, a temperature of 30 °C and a concentration of 15 wt% – the greenhouse temperature and relative humidity are maintained between optimal ranges for typical crops. This concentration of 15 wt% requires a 9-stage NF regenerator which has a maximum electric power requirement of 6.212 kW, a specific work of 309.6 kJ/kg and a yearly average *COP* of 12.4. The electric power requirement of the NF regenerator can be fully provided by PV collectors covering half the greenhouse roof area, while generating excess electricity for other purposes besides cooling. A 9-stage regenerator is required because commercial NF membranes have a burst pressure of ~ 40 bar [4,44–48]. However, NF membranes with burst pressures of 55 bar would give the same results using only 4 stages, decreasing the complexity, size and cost of the NF regenerator. Specifically, the 4-stage NF regenerator would have a maximum electric power requirement of 6.274 kW, a specific work of 312.6 kJ/kg and a yearly average *COP* of 12.4. Therefore, the fabrication of more robust NF membranes with rejections of 10–40 % is an important topic for future research.

CRediT authorship contribution statement

P. Pasqualin: Writing – review & editing, Data curation, Investigation, Visualization. **P.A. Davies:** Supervision, Conceptualization.

Declaration of Competing Interest

The authors declare that they have no known competing financial interests or personal relationships that could have appeared to influence the work reported in this paper.

Acknowledgements

P. Pasqualin acknowledges funding from the School of Engineering, University of Birmingham, UK.

Appendix A. Equations to calculate ET_c

The equations to calculate the parameters of Eq. (25) are presented here; Eqs. (A.1)-(A.8) taken from Acquah et al. [64].

$$\lambda = 2501 - 2.361T_{\text{cool}} \tag{A.1}$$

$$\Delta = \frac{4042.9 \times \exp\left(23.57712 - \frac{4042.9}{T_{\text{cool}}+237.57}\right)}{10^3\left(T_{\text{cool}} + 237.57\right)^2} \tag{A.2}$$

$$VPD = 4042.9 \times \exp\left(23.57712 - \frac{4042.9}{T_{\text{cool}} + 237.57}\right) \times \left(1 - \frac{RH_{\text{cool}}}{100}\right) \tag{A.3}$$

$$\rho_{\text{Air}} = \frac{10^5}{287(T_{\text{cool}} + 273.15)} \tag{A.4}$$

$$r_{\text{R}} = \frac{10^3 \rho_{\text{Air}}\, c_{\text{p,Air}}}{4 \times \sigma_{\text{S-B}}\left(T_{\text{cool}} + 273.15\right)^3} \tag{A.5}$$

$$r_{\text{a}} = \frac{665}{1 + 0.54U_{\text{Air}}} \tag{A.6}$$

$$R_{\text{n}} = 0.0031I\tau[1 - \exp(-0.7LAI)] \tag{A.7}$$

$$r_{\text{c}} = \frac{2}{LAI(108.5 + 660 \times \exp(-9I))} \tag{A.8}$$

where U_{Air} is the air speed [m/s], RH_{cool} is the relative humidity of the cool air leaving the dehumidifier [%] and $\sigma_{\text{S-B}}$ is the constant of Stefan–Boltzmann equal to 5.67 × 10^{-8} W/(m^2 K^4).

Appendix B:. Modelling of the dehumidifier

The moisture absorption is a natural process which equilibrates the vapour pressures of the air and the LD, meaning that a higher dehumidification effectiveness is attained when the vapour pressure difference is high. For example, air at $T = 30$ °C and $RH = 70$ % has a vapour pressure (P_{vap}) of 2.972 kPa. On the other hand, $CaCl_2$ at temperatures of 25 and 35 °C and weight concentrations of 25 and 35 wt% has vapour pressures between 1.614 and 4.235 kPa [65] (Table B.1).

The dehumidifier model calculates the outlet conditions of the air and the LD as it follows:

Table B.1
Vapour pressure of $CaCl_2$ ($P_{vap,CaCl2}$) [kPa] at temperatures of 25 and 35 °C and weight concentrations of 25 and 35 wt% based on Patil et al. [65].

$P_{vap,CaCl2}$ [kPa][1]	Temperature [°C]	
Concentration [wt.%]	25	35
25	2.365	4.235
35	1.614	2.941

[1] If higher than the air, then the air will absorb moisture from the LD.

(1) Fix the input conditions of the air and LD.
- Air
  - $\dot{m}_{Air}^{in}$, mass flow of air entering the dehumidifier [kg/s]
  - T_{Air}^{in}, temperature of air entering the dehumidifier [°C]
  - RH_{Air}^{in}, relative humidity of air entering the dehumidifier [-]
  - T_{Air}^{in} and RH_{Air}^{in} allow to calculate the enthalpy (h_{Air}^{in}) and the absolute humidity (x_{Air}^{in})
  - $\dot{m}_{d,Air}^{in}$, mass flow of dry air entering the dehumidifier [kg/s]

$$\dot{m}_{d,Air}^{in} = \dot{m}_{Air}^{in}\left(1 - \frac{1}{10^{-3}x_{Air}^{in} + 1}\right) \tag{B.1}$$

- $\dot{m}_{v,Air}^{in}$, mass flow of moisture entering the dehumidifier [kg/s]

$$\dot{m}_{v,Air}^{in} = \dot{m}_{Air}^{in} - \dot{m}_{d,Air}^{in} \tag{B.2}$$

- LD
  - $\dot{m}_{LD}^{in}$, mass flow of LD entering the dehumidifier [kg/s]
  - T_{LD}^{in}, temperature of LD entering the dehumidifier [°C]
  - wt_{LD}^{in}, weight concentration of LD entering the dehumidifier [–]

$$\varepsilon_{deh} = -0.0333\left(T_{Air}^{in} - T_{LD}^{in}\right) + 0.9667 \tag{B.3}$$

(2) Calculate the effectiveness of the dehumidifier (ε_{deh}).

The proposed equation for ε_{deh} gave results in agreement with a dehumidifier which was tested in an R&D greenhouse at KAUST (Saudi Arabia) and the experimental results of Koronaki et al. [66]. Future studies could improve the calculation of ε_{deh} by also accounting for the geometry of the dehumidifier and other operating parameters.

(3) Assume that the outlet LD temperature (T_{LD}^{in}) is equal to the inlet temperature and calculate the outlet air temperature (T_{Air}^{out}) as the mean temperature of the LD. This calculation is used by TRNSYS software [67] and agrees with Koronaki et al. experiments [66].

$$T_{Air}^{out} = (T_{LD}^{out} + T_{LD}^{in})/2 \tag{B.4}$$

(4) Assume that the outlet vapour pressures of the air ($P_{vap,Air}^{out}$) and the LD ($P_{vap,LD}^{out}$) are equal to their inlet $P_{vap,Air}^{in}$ and $P_{vap,LD}^{in}$, respectively. The $P_{vap,LD}$ is calculated based on [65] while $P_{vap,air}$ as:

$$P_{vap,air} = 4042.9 \times \exp\left(23.57712 - \frac{4042.9}{T_{Air} + 237.57}\right) \times \left(\frac{RH_{Air}}{100}\right) \tag{B.5}$$

(5) Start a while loop for $\dot{m}_v$ going from 0 to $\dot{m}_{v,Air}^{in}$ with an increment step $\dot{m}_{v,step}$. By increasing $\dot{m}_v$, the vapour pressures of the air and the LD change. The while loop is implemented until the vapour pressure difference becomes zero. Therefore, the while loop is as follows: while $P_{vap,LD}^{out} < P_{vap,Air}^{out}$

(a) Assumption of the new moisture absorption rate [kg/s]:

$$\dot{m}_{v,new} = \dot{m}_v + \dot{m}_{v,step} \tag{B.6}$$

(b) Calculation of the outlet flows of air ($\dot{m}_{Air}^{out}$) and LD ($\dot{m}_{LD}^{out}$):

$$\dot{m}_{air}^{out} = \dot{m}_{air}^{in} - \dot{m}_{v,step} \tag{B.7}$$

$$\dot{m}_{LD}^{out} = \dot{m}_{LD}^{in} + \dot{m}_{v,step} \tag{B.8}$$

(c) Calculation of the new outlet LD weight concentration [wt.%]:

$$wt_{\mathrm{LD}}{}^{\mathrm{out}} = \frac{\dot{m}_{\mathrm{LD}}{}^{\mathrm{in}} \times wt_{\mathrm{LD}}{}^{\mathrm{in}}}{\dot{m}_{\mathrm{LD}}{}^{\mathrm{in}} + \dot{m}_{\mathrm{v,new}}} \tag{B.9}$$

(d) Calculation of the outlet air absolute humidity [g_v/kg_a]:

$$x_{\mathrm{air}}{}^{\mathrm{out}} = 10^3 \frac{\dot{m}_{\mathrm{v,Air}}{}^{\mathrm{in}} - \dot{m}_{\mathrm{v,new}}}{(\dot{m}_{\mathrm{Air}}{}^{\mathrm{in}} - \dot{m}_{\mathrm{v,Air}}{}^{\mathrm{in}})} \tag{B.10}$$

(e) Knowing $T_{\mathrm{Air}}{}^{\mathrm{out}}$ and $x_{\mathrm{Air}}{}^{\mathrm{out}}$, the enthalpy ($h_{\mathrm{Air}}{}^{\mathrm{out}}$) and the relative humidity ($RH_{\mathrm{Air}}{}^{\mathrm{out}}$) of the outlet air can be calculated. Then, the heat difference between the inlet and outlet air (Q_{Air}) [kW] is calculated as:

$$Q_{\mathrm{Air}} = \dot{m}_{\mathrm{Air}}{}^{\mathrm{in}} h_{\mathrm{Air}}{}^{\mathrm{in}} - \dot{m}_{\mathrm{Air}}{}^{\mathrm{out}} h_{\mathrm{Air}}{}^{\mathrm{out}} \tag{B.11}$$

(f) Calculation of the heat capacity of the inlet LD $\left(c_{\mathrm{p,LD}}{}^{\mathrm{in}}\right)$ and outlet LD $\left(c_{\mathrm{p,LD}}{}^{\mathrm{out}}\right)$. The heat capacity depends on the LD temperature and weight concentration. For $CaCl_2$, this can be calculated using data from [68]. Then, the outlet LD temperature $T_{\mathrm{LD}}{}^{\mathrm{out}}$ [°C] is calculated as:

$$T_{\mathrm{LD}}{}^{\mathrm{out}} = \frac{Q_{\mathrm{Air}} + \dot{m}_{\mathrm{LD}}{}^{\mathrm{in}} c_{\mathrm{p,LD}}{}^{\mathrm{in}} (T_{\mathrm{LD}}{}^{\mathrm{in}} + 273.15)}{\dot{m}_{\mathrm{LD}}{}^{\mathrm{out}} c_{\mathrm{p,LD}}{}^{\mathrm{out}}} - 273.15 \tag{B.12}$$

(g) Knowing $T_{\mathrm{LD}}{}^{\mathrm{out}}$ and $wt_{\mathrm{LD}}{}^{\mathrm{out}}$, the outlet LD vapour pressure ($P_{\mathrm{vap,LD}}{}^{\mathrm{out}}$) can be calculated, based on [65].

(h) Calculation of the ideal outlet air temperature ($T_{\mathrm{Air,id}}{}^{\mathrm{out}}$) [°C] and the real air temperature accounting for the effectiveness of the dehumidifier ($T_{\mathrm{Air}}{}^{\mathrm{out}}$) [°C].

$$T_{\mathrm{Air,id}}{}^{\mathrm{out}} = (T_{\mathrm{LD}}{}^{\mathrm{out}} + T_{\mathrm{LD}}{}^{\mathrm{in}})/2 \tag{B.13}$$

$$T_{\mathrm{Air}}{}^{\mathrm{out}} = T_{\mathrm{Air}}{}^{\mathrm{in}} - \varepsilon_{\mathrm{deh}} (T_{\mathrm{Air}}{}^{\mathrm{in}} - T_{\mathrm{Air,id}}{}^{\mathrm{out}}) \tag{B.14}$$

(i) Knowing $T_{\mathrm{Air}}{}^{\mathrm{out}}$ and $x_{\mathrm{Air}}{}^{\mathrm{out}}$ the outlet air vapour pressure ($P_{\mathrm{vap,air}}{}^{\mathrm{out}}$) can be calculated. Note that $T_{\mathrm{Air}}{}^{\mathrm{out}}$ is called $T_{\mathrm{out}}{}^{\mathrm{deh}}$ in the modelling section. Here it was renamed to distinguish it from $T_{\mathrm{LD}}{}^{\mathrm{out}}$.

(6) If $P_{\mathrm{vap,LD}}{}^{\mathrm{out}} = P_{\mathrm{vap,Air}}{}^{\mathrm{out}}$, end the while loop, if not, return to the beginning of the while loop. With this method, the outlet air temperature may converge to a certain value (Fig. B.1), but it may also never converge. When $\dot{m}_{\mathrm{LD}}{}^{\mathrm{in}}$ is four times less than $\dot{m}_{\mathrm{LD}}{}^{\mathrm{in}}$, this method does not converge.

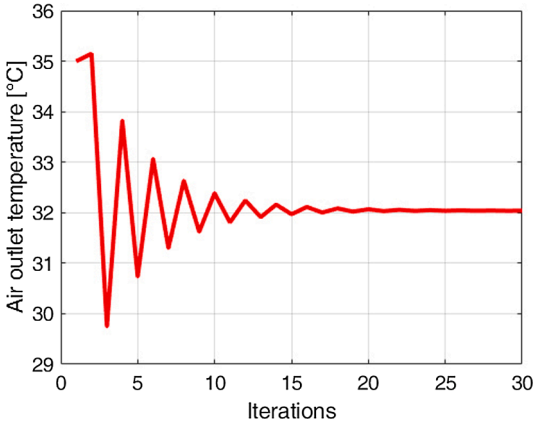

Fig. B.1. Example of convergence of the outlet air temperature from the dehumidifier.

Appendix C. Supplementary material

Supplementary data to this article can be found online at https://doi.org/10.1016/j.applthermaleng.2022.119057.

References

[1] P.A. Davies, A solar cooling system for greenhouse food production in hot climates, Sol. Energy 79 (6) (2005) 661–668.
[2] D. Misra, S. Ghosh, Evaporative cooling technologies for greenhouses: a comprehensive review, Agric. Eng. Int.: CIGR J. 20 (1) (2018) 1–15.
[3] A. Gurubalan, M. Maiya, P.J. Geoghegan, A comprehensive review of liquid desiccant air conditioning system, Appl. Energy 254 (2019) 113673.
[4] M.M. Rafique, P. Gandhidasan, H.M.S. Bahaidarah, Liquid desiccant materials and dehumidifiers–A review, Renew. Sustain. Energy Rev. 56 (2016) 179–195.
[5] C. Stanghellini, B. Oosfer, E. Heuvelink, *Greenhouse horticulture: technology for optimal crop production*. 2019: Wageningen Academic Publishers.
[6] M. Teitel, J. Montero, E. Baeza, Greenhouse design: Concepts and trends, in: *International Symposium on Advanced Technologies and Management Towards Sustainable Greenhouse Ecosystems: Greensys*, 2011, p. 952.
[7] H.C. Duong, A.J. Ansari, L.D. Nghiem, H.T. Cao, T.D. Vu, T.P. Nguyen, Membrane Processes for the Regeneration of Liquid Desiccant Solution for Air Conditioning, Curr. Pollut. Rep. 5 (4) (2019) 308–318.
[8] S. Bouzenada, L. Frainkin, A. Léonard, Experimental investigation on vapor pressure of desiccant for air conditioning application, Proc. Comput. Sci. 109 (2017) 817–824.
[9] R. Lefers, N.M.S. Bettahalli, S.P. Nunes, N. Fedoroff, P.A. Davies, TorOve Leiknes, Liquid desiccant dehumidification and regeneration process to meet cooling and freshwater needs of desert greenhouses, Desalin. Water Treat. 57 (48-49) (2016) 23430–23442.
[10] R. Qi, C. Dong, L.-Z. Zhang, A review of liquid desiccant air dehumidification: from system to material manipulations, Energy Build. 215 (2020) 109897, https://doi.org/10.1016/j.enbuild.2020.109897.
[11] T. Tong, M. Elimelech, The global rise of zero liquid discharge for wastewater management: drivers, technologies, and future directions, Environ. Sci. Technol. 50 (13) (2016) 6846–6855.
[12] G. Lychnos, P.A. Davies, Modelling and experimental verification of a solar-powered liquid desiccant cooling system for greenhouse food production in hot climates, Energy 40 (1) (2012) 116–130.
[13] H.C. Duong, F.I. Hai, A. Al-Jubainawi, Z. Ma, T. He, L.D. Nghiem, Liquid desiccant lithium chloride regeneration by membrane distillation for air conditioning, Sep. Purif. Technol. 177 (2017) 121–128.
[14] R. Lefers, N.M.S. Bettahalli, N. Fedoroff, S.P. Nunes, TorOve Leiknes, Vacuum membrane distillation of liquid desiccants utilizing hollow fiber membranes, Sep. Purif. Technol. 199 (2018) 57–63.
[15] A.S. Rattner, A.K. Nagavarapu, S. Garimella, T.F. Fuller, Modeling of a flat plate membrane-distillation system for liquid desiccant regeneration in air-conditioning applications, Int. J. Heat Mass Transf. 54 (15-16) (2011) 3650–3660.
[16] J. Zhou, F. Wang, N. Noor, X. Zhang, An experimental study on liquid regeneration process of a liquid desiccant air conditioning system (LDACs) based on vacuum membrane distillation, Energy 194 (2020) 116891.
[17] J. Zhou, X. Zhang, W. Su, B.o. Sun, Performance analysis of vacuum membrane distillation regenerator in liquid desiccant air conditioning system, Int. J. Refrig 102 (2019) 112–121.
[18] F.A. Al-Sulaiman, P. Gandhidasan, S.M. Zubair, Liquid desiccant based two-stage evaporative cooling system using reverse osmosis (RO) process for regeneration, Appl. Therm. Eng. 27 (14-15) (2007) 2449–2454.
[19] A. Al-Jubainawi, Z. Ma, Y.i. Guo, L.D. Nghiem, P. Cooper, W. Li, Factors governing mass transfer during membrane electrodialysis regeneration of LiCl solution for liquid desiccant dehumidification systems, Sustain. Cities Soc. 28 (2017) 30–41.
[20] Q. Cheng, W. Pei, Performance comparison on different liquid desiccants in the liquid desiccant air-conditioning using electrodialysis regeneration: LiCl and LiBr aqueous solutions, Int. J. Refrig 107 (2019) 1–10.
[21] Y.i. Guo, Z. Ma, A. Al-Jubainawi, P. Cooper, L.D. Nghiem, Using electrodialysis for regeneration of aqueous lithium chloride solution in liquid desiccant air conditioning systems, Energy Build. 116 (2016) 285–295.
[22] W. Pei, Q. Cheng, S. Jiao, L. Liu, Performance evaluation of the electrodialysis regenerator for the lithium bromide solution with high concentration in the liquid desiccant air-conditioning system, Energy 187 (2019) 115928.
[23] B.o. Sun, X. Zhang, Experimental study on liquid desiccant regeneration by photovoltaic electrodialysis, Energy Proc. 158 (2019) 959–964.
[24] C. Fritzmann, J. Löwenberg, T. Wintgens, T. Melin, State-of-the-art of reverse osmosis desalination, Desalination 216 (1-3) (2007) 1–76.
[25] L.F. Greenlee, D.F. Lawler, B.D. Freeman, B. Marrot, P. Moulin, Reverse osmosis desalination: water sources, technology, and today's challenges, Water Res. 43 (9) (2009) 2317–2348.
[26] M. Elimelech, W.A. Phillip, The Future of Seawater Desalination: Energy, Technology, and the Environment, Science 333 (6043) (2011) 712–717.
[27] P. Pasqualin, R. Lefers, S. Mahmoud, P.A. Davies, Comparative review of membrane-based desalination technologies for energy-efficient regeneration in liquid desiccant air conditioning of greenhouses, Renew. Sustain. Energy Rev. 154 (2022) 111815.
[28] *Toray Innovation by Chemistry, Standard SWRO TM800M.* 2019. Retrieved from https://www.toraywater.com/products/ro/pdf/TM800M.pdf.
[29] *Hydranautics Nitto Group Company, SWC4 MAX. Accessed: 08-01-2022.* 2019. Retrieved from https://membranes.com/wp-content/uploads/Documents/Element-Specification-Sheets/RO/SWC/SWC4-MAX.pdf.
[30] A. AlTaee, A.O. Sharif, Alternative design to dual stage NF seawater desalination using high rejection brackish water membranes, Desalination 273 (2-3) (2011) 391–397.
[31] Z. Wang, A. Deshmukh, Y. Du, M. Elimelech, Minimal and zero liquid discharge with reverse osmosis using low-salt-rejection membranes, Water Res. 170 (2020) 115317.
[32] D.M. Davenport, A. Deshmukh, J.R. Werber, M. Elimelech, High-pressure reverse osmosis for energy-efficient hypersaline brine desalination: current status, design considerations, and research needs, Environ. Sci. Technol. Lett. 5 (8) (2018) 467–475.
[33] M.D. Afonso, M.N. de Pinho, Transport of MgSO4, MgCl2, and Na2SO4 across an amphoteric nanofiltration membrane, J. Membr. Sci. 179 (1-2) (2000) 137–154.
[34] Z.V.P. Murthy, L.B. Chaudhari, Rejection behavior of nickel ions from synthetic wastewater containing Na2SO4, NiSO4, MgCl2 and CaCl2 salts by nanofiltration and characterization of the membrane, Desalination 247 (1-3) (2009) 610–622.
[35] W. Li, C. Shi, A. Zhou, X. He, Y. Sun, J. Zhang, A positively charged composite nanofiltration membrane modified by EDTA for LiCl/MgCl2 separation, Sep. Purif. Technol. 186 (2017) 233–242.
[36] P.A. Davies, P.R. Knowles, Seawater bitterns as a source of liquid desiccant for use in solar-cooled greenhouses, Desalination 196 (1-3) (2006) 266–279.
[37] *ThermoFisher SCIENTIFIC, SAFETY DATA SHEET, Product Description: Lithium chloride, anhydrous. Accessed: 29-04-2022.* Retrieved from https://www.fishersci.co.uk/store/msds?partNumber=12367083&productDescription=1KG+Lithium+chloride%2C+99%25%2C+extra+pure&countryCode=GB&language=en.
[38] *ThermoFisher SCIENTIFIC, SAFETY DATA SHEET, Product Description: Lithium bromide. Accessed: 29-04-2022.* Retrieved from https://www.fishersci.co.uk/store/msds?partNumber=15234674&productDescription=10KG+Lithium+bromide%2C+99%2B%25%2C+for+analysis%2C+anhydrou&countryCode=GB&language=en.
[39] *ThermoFisher SCIENTIFIC, SAFETY DATA SHEET, Product Description: Calcium chloride. Accessed: 29-04-2022.* Retrieved from https://www.alfa.com/en/msds/?language=EN&subformat=CLP1&sku=L13191.
[40] G. Lychnos, *Feasibility of a solar panel-powered liquid desiccant cooling system for greenhouses*. 2010, Aston University.
[41] N.H. Abu-Hamdeh, K.H. Almitani, Solar liquid desiccant regeneration and nanofluids in evaporative cooling for greenhouse food production in Saudi Arabia, Sol. Energy 134 (2016) 202–210.
[42] C. Kittas, T. Bartzanas, A. Jaffrin, Temperature gradients in a partially shaded large greenhouse equipped with evaporative cooling pads, Biosyst. Eng. 85 (1) (2003) 87–94.
[43] C. Kittas, T. Bartzanas, A. Jaffrin, Greenhouse evaporative cooling: measurement and data analysis, Trans. ASAE 44 (3) (2001) 683.
[44] T.L. Oladosu, A.T. Baheta, A.N. Oumer, Desiccant solutions, membrane technologies, and regeneration techniques in liquid desiccant air conditioning system, Int. J. Energy Res. 45 (6) (2021) 8420–8447.
[45] W. Li, Y. Pan, Y.e. Yao, M. Dong, Modeling and parametric study of the ultrasonic atomization regeneration of desiccant solution, Int. J. Heat Mass Transf. 127 (2018) 687–702.
[46] S. Bouzenada, C. McNevin, S. Harrison, A. Kaabi, Performance of a liquid desiccant air-conditioner driven by evacuated-tube, flat-plate, or hybrid solar thermal arrays, Energy Build. 117 (2016) 53–62.
[47] W. Li, Y. Yao, Thermodynamic analysis of internally-cooled membrane-based liquid desiccant dehumidifiers of different flow types, Int. J. Heat Mass Transf. 166 (2021) 120802.
[48] Y. Yao, W. Li, Y. Hu, Modeling and performance investigation on the counter-flow ultrasonic atomization liquid desiccant regenerator, Appl. Therm. Eng. 165 (2020) 114573.
[49] B. Huang, K. Pu, P. Wu, D. Wu, J. Leng, Design, selection and application of energy recovery device in seawater desalination: A review, Energies 13 (16) (2020) 4150.
[50] C. Stanghellini, Transpiration of greenhouse crops: an aid to climate management. 1987, IMAG.
[51] J. Prenger, R. Fynn, R. Hansen, A comparison of four evapotranspiration models in a greenhouse environment, Trans. ASAE 45 (6) (2002) 1779.
[52] F. Villarreal-Guerrero, M. Kacira, E. Fitz-Rodríguez, C. Kubota, G.A. Giacomelli, R. Linker, A. Arbel, Comparison of three evapotranspiration models for a greenhouse cooling strategy with natural ventilation and variable high pressure fogging, Sci. Hortic. 134 (2012) 210–221.
[53] E.B. Smith, *Basic chemical thermodynamics*. Vol. 35. 2004: Imperial College Press.
[54] M.R. Conde, Properties of aqueous solutions of lithium and calcium chlorides: formulations for use in air conditioning equipment design, Int. J. Therm. Sci. 43 (4) (2004) 367–382.
[55] *CAT PUMPS (U.K.) LTD, Pump Catalogue. Accessed: 08-01-2022.* 2018. Retrieved from http://www.www.catpumps.co.uk/products/pdfs/20043%20CAT%20Pump%20Catalog%20UK%2099CATUK001E.pdf.
[56] Y.A. Cengel, *Introduction to thermodynamics and heat transfer*. Vol. 846. 1997: McGraw-Hill New York.
[57] *BLD Solar Europe GmbH. Datasheet Photovoltaic Modules. Accessed: 08-01-2022.* Retrieved from http://eprints.polsri.ac.id/4627/11/Solar%20Cell.pdf.
[58] P.A. Davies, G. Zaragoza, Ideal performance of a self-cooling greenhouse, Appl. Therm. Eng. 149 (2019) 502–511.
[59] GEOCLIMA smart HVAC Solutions, TECHNICAL Data Sheet, GHA FC, AIR COOLED CHILLER WITH SCREW COMPRESSORS, AXIAL FANS AND FREE COOLING FOR OUTDOOR INSTALLATION. Accessed: 04-05-2022. Retrieved from https://www.cooltherm.co.uk/uploads/files/SelDocsGeo/gha.pdf.
[60] GEOCLIMA smart HVAC Solutions, TECHNICAL Data Sheet, VHH, WATER COOLED CHILLER WITH SCROLL OR RECIPROCATING COMPRESSORS FOR INDOOR INSTALLATION. Accessed: 04-05-2022. Retrieved from https://www.cooltherm.co.uk/uploads/files/SelDocsGeo/vhh.pdf.

[61] *DAIKIN, Air cooled scroll inverter chiller EWAQ-BAWN/BAWP. Accessed: 04-05-2022.* Retrieved from https://www.daikin.eu/content/dam/document-library/catalogues/as/air-cooled-chiller/ewaq-bawn/EWAQ-BAWN_BAWP%20Product%20flyer_ECPEN15-422_1_Product%20Catalogues_English.pdf.

[62] M. Salikandi, B. Ranjbar, E. Shirkhan, S.S. Priya, I. Thirunavukkarasu, K. Sudhakar, Recent trends in liquid desiccant materials and cooling systems: application, performance and regeneration characteristics, J. Build. Eng. 33 (2021) 101579.

[63] R.u. Yang, P.-L. Wang, The optimum glazing height of a glazed solar collector/regenerator for open-cycle absorption cooling, Energy 19 (9) (1994) 925–931.

[64] S. Joe Acquah, H. Yan, C. Zhang, G. Wang, B. Zhao, H. Wu, H. Zhang, Application and evaluation of Stanghellini model in the determination of crop evapotranspiration in a naturally ventilated greenhouse, Int. J. Agric. Biol. Eng. 11 (6) (2018) 95–103.

[65] K.R. Patil, A.D. Tripathi, G. Pathak, S.S. Katti, Thermodynamic properties of aqueous electrolyte solutions. 2. Vapor pressure of aqueous solutions of sodium bromide, sodium iodide, potassium chloride, potassium bromide, potassium iodide, rubidium chloride, cesium chloride, cesium bromide, cesium iodide, magnesium chloride, calcium chloride, calcium bromide, calcium iodide, strontium chloride, strontium bromide, strontium iodide, barium chloride, and barium bromide, J. Chem. Eng. Data 36 (2) (1991) 225–230.

[66] I.P. Koronaki, R.I. Christodoulaki, V.D. Papaefthimiou, E.D. Rogdakis, Thermodynamic analysis of a counter flow adiabatic dehumidifier with different liquid desiccant materials, Appl. Therm. Eng. 50 (1) (2013) 361–373.

[67] TESSLibs 17 Component Libraries for the TRNSYS Simulation Environment, Volume 06, HVAC Library Mathematical Reference, TESS – Thermal Energy Systems Specialists. Accessed: 08-01-2022. Retrieved from http://www.trnsys.com.

[68] *Occidental Chemical Corporation. Calcium Chloride A Guide to Physical Properties. Accessed: 08-04-2022.*